Nonlinear pattern dynamics in Josephson-junction arrays

J. Oppenländer, G. Dangelmayr, and W. Güttinger
Institut für Theoretische Physik, Universität Tübingen, Köstlinstrasse 6, D-72074 Tübingen, Germany
(Received 28 September 1995; revised manuscript received 7 March 1996)

The dynamics of a two-dimensional array of Josephson junctions under an external load is shown to be equivalent to that of a one-dimensional nonlinear chain of nonidentical, globally, and nonuniformly coupled oscillators. This allows us to determine the dynamical states and collective spatiotemporal patterns the array exhibits in response to varying initial conditions, input patterns, coupling strengths, and bias current. When the bias current goes through critical values, successive bifurcations activate spatially distinct, coupled oscillatory compartments in the array, where semirotating, whirling, and quasiperiodic and aperiodic states coexist, and induce staircase current-voltage characteristics. Classical and vortex-induced row switching phenomena, stable families of frequency synchronized and phase-locked states, subharmonics in compartment couplings, stochastic jumps, and hysteresis loops are deduced, and sequences of input patterns are shown to be dynamically storable in the array's attractors. The dynamical formation of oscillatory compartments is also a general feature of three-dimensional Josephson-junction networks. Coherent microwave radiation emission is possible only for specific input patterns or by using symmetry-breaking array architectures. The theoretical predictions are in close agreement with the dynamics recently observed in low-temperature scanning electron microscopy experiments. [S0163-1829(96)08126-X]

I. INTRODUCTION

The objective of this paper is to develop a comprehensive theoretical framework for the description of two-dimensional Josephson-junction arrays which is capable of explaining quantitatively the dynamical states and spatiotemporal patterns recently observed in experiments and provides insight into the underlying nonlinear dynamics.

The increasing contemporary interest in the dynamics of two-dimensional (2D) Josephson-junction arrays derives from the technological potential these systems hold as coherently radiating on-chip high-frequency sources, magnetic field sensors, and kryoelectronic switching circuits.[1–4] In addition, layered 2D arrays and 3D lattices of Josephson junctions play an important role in modeling high-temperature superconductors.[5] On the other hand, operating massively parallel, Josephson networks possess both pattern generating and recognizing capabilities depending on the system's coupling architecture and so can be used in the design of dynamical devices for ultrafast signal processing.

Experimental and theoretical studies of phase oscillations in one-dimensional (1D) uniform Josephson arrays, in which all junctions are globally coupled with each other under an external load, have demonstrated the feasibility of phase-locked coherent oscillations needed for high output power.[6,7,9–12] However, because of the complex nonlinear dynamics associated with the many interacting degrees of freedom in 2D and 3D Josephson networks, our understanding of the possibility of phase and frequency synchronization and of the dynamical states observed in such systems is still far from being satisfactory.[9,13–15] To achieve stable states of in-phase junction oscillations seems to require additional mechanisms to be built into the arrays. On the other hand, recent spatial imaging measurements using low-temperature scanning electron microscopy (LTSEM) techniques[16,17] have revealed a rich variety of dynamical patterns in 2D Josephson-junction arrays, with a nonlinear theory still missing.

Since Josephson arrays represent discrete nonlinear dynamical systems for the set of phase differences across the junction barriers, the central problem to be addressed here is to model these systems by networks of nonlinear oscillators whose collective spatiotemporal patterns, such as frequency and phase synchronization, self-stabilization, and compartment formation, reproduce the experimental findings quantitatively.

In Sec. II we show that the nonlinear dynamical equations for the phase oscillations of a 2D Josephson-junction array coupled to an external load can be transformed into an equation system for a one-dimensional chain of nonlinear, globally, and nonuniformly coupled, nonidentical oscillators. From this we determine, in Sec. III, the spatiotemporal patterns and dynamical states the array exhibits in response to varying input patterns, coupling strengths, bias current, and external probes. As the dc bias current increases beyond the critical current, the dynamics is governed by a succession of bifurcations which activate spatially distinct, coupled compartments of oscillators with different frequencies in the array in which fixed points, semirotating, whirling, and quasiperiodic and aperiodic states coexist and interact. If the current goes through critical values, the formation of oscillatory compartments induces successive staircase steps in the current-voltage characteristics. For sufficiently large bias current, the compartments merge into a single block and the existence of constants of motion implies that the current-voltage characteristics become linear with all array junctions oscillating with the same frequency in an, in general, incoherent phase-locked state. To achieve coherence, the array's dynamical symmetry must be broken explicitly, either by applying specific inputs, e.g., by microwave injection, or by using special coupling schemes, e.g., hierarchic-modular array architectures.[18]

It is shown that the mechanisms described above give rise to a variety of experimentally observable macroscopic quantum phenomena, in particular to frequency-synchronized families of phase-locked oscillations, classical and vortex-induced row switching due to energy transport between compartments, and voltage drops, subharmonics, stochastic jumps, and hysteresis loops in the current voltage characteristics. Compartment formation is also revealed in three-dimensional Josephson networks used to model high-temperature superconductors. The striking dependence of the network dynamics on the initial conditions imposed on the Josephson array by given input patterns, such as applied microwave signals or electron beams in spatially resolved LTSEM-based measurements, is analyzed. Since the currents generated by input patterns change the array's coupling strengths in a dynamical process, the network can self-organize its oscillatory behavior and, operating as a current-pattern to voltage-pattern transducer, store different input patterns in the array's attractors. We confirm our findings by numerically integrating the array's equation system and test the stability of the patterns against noise and parameter spreads.

In Sec. IV we summarize our results and discuss implications for pattern sequences, coherent radiation, and layered networks of Josephson-junction arrays. The theoretical predictions are in full agreement with the dynamical patterns recently observed in LTSEM experiments on rectangular arrays of underdamped and overdamped Josephson junctions[20,21] and reproduce the measured data with high accuracy.

II. ARRAY EQUATIONS

In this section we set up the dynamical equation system for the two-dimensional rectangular array of identical Josephson junctions shown in Fig. 1(a) and discuss its basic properties. The array is shunted by a load to provide global coupling of the junctions symbolized by crosses. In experiments bus-bar resistors are used on top and bottom to ensure homogeneous input currents fed into the columns of the network. The column index is denoted by $i=1,\ldots,M$ (from left to right) and the row index by $j=1,\ldots,N+1$ (from top to bottom), each cross being represented by the resistively and capacitively shunted junction (RCSJ) circuit of Fig. 1(b). Each junction on a vertical branch (vertical junctions) is marked by the node above, each junction on a horizontal branch (horizontal junctions) by the node to its left. The size of the array is characterized by the number of vertical junctions $(N\times M)$ so that the total number of junctions in the array is $NM+(N+1)(M-1)$ and the total number of unit cells equals $N(M-1)$. We neglect magnetic field and inductance effects. In Ref. 9 it was shown that this is justified for arrays with ground planes and in Ref. 20 no qualitative difference in the experimentally observed spatiotemporal patterns for arrays with and without a ground plane was found. The applied dc current I_A is fed into the array at the top and subtracted at the bottom [Fig. 1(a)]. Hence, current conservation for the sum of the currents through the vertical junctions in one row implies that for the horizontal junctions three different types of dynamical states can be distinguished depending on the current I_{ij}^H flowing through a single horizontal junction: (i) All horizontal junctions are totally inactive, i.e., $I_{ij}^H=0\ \forall i,j$. (ii) For each horizontal junction the current remains less than its critical current I_c, i.e., $I_{ij}^H<I_c\ \forall i,j$, so that the junctions exhibit the dc Josephson effect. (iii) The input current I_A is distributed over the array in such a way that the horizontal junctions exhibit the dc $(I_{ij}^H<I_c)$ or the ac $(I_{ij}^H>I_c)$ Josephson effect when I_A is sufficiently high. According to the general Josephson relations, for type (i) and (ii) current distributions there exists no voltage drop between different array columns so that the phase differences Φ_{ij}^H of the horizontal junctions remain bounded. Case (i) is nongeneric because for real physical systems even small imperfections or perturbations lead to horizontal currents, so that (i) and (ii) should be dealt with together. The above classification is also indicated by the results of recent spatially resolved measurements on 2D arrays.[16,17,20,21] These experiments show that, if the input current is nearly homogeneously fed into and subtracted from the array by using standard bus-bar resistors,[3,9] the horizontal junctions do not oscillate, implying that there is no voltage drop in the

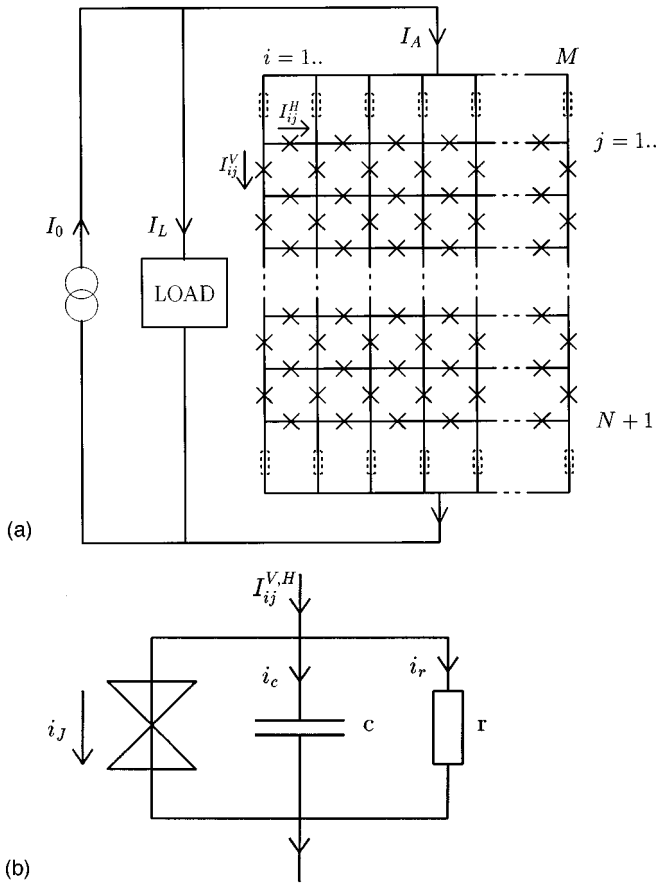

FIG. 1. (a) Geometry of a 2D Josephson-junction array with a parallel shunted load. The junctions are indicated by crosses and labeled by their column index $i=1,\ldots,M$ (from left to right) and their row index $j=1,\ldots,N+1$ (from top to bottom). I_{ij}^V and I_{ij}^H denote the current through the vertical and horizontal junctions, respectively. On top and bottom of the array experimentally used bus-bar resistors are sketched which provide homogeneous array input and output currents. (b) RCSJ circuit for a single junction. $I_{ij}^{V,H}$ is the current from a network node, i_J the Josephson supercurrent, and i_c and i_r are the currents through capacitor and resistor.

direction perpendicular to the bias current. In addition, even if the array is influenced by external microwave irradiation to which the vertical junctions lock in their phases, the horizontal junctions do not switch into the voltage state and so do not oscillate.[20] Consequently case (iii) does not apply to these experiments since $I_{ij}^H > I_c$ would imply oscillations. On the other hand it is also experimentally known that the vertical junctions in general oscillate incoherently,[3,9] so that horizontal currents necessarily must exist ($I_{ij}^H \neq 0$). Therefore, the observed collective dynamical patterns must be the result of type (ii) current distributions. The spatiotemporal patterns the array exhibits for type (iii) current distributions are qualitatively different from those for types (i) and (ii) and are extremely sensitive to the boundary conditions applied to the array such as strongly nonhomogeneous input currents. This is a consequence of the fact that the dynamics of the array is restricted by the geometric flux quantization constraint which implies that the sum over all junction phase differences arround any closed loop within the network must be an integer multiple of 2π [Eq. (9)]. As we will show below, array equations for type (ii) current distributions which take into account this flux quantization condition and reproduce the experimental data can be formulated in terms of a nonlinear chain of coupled oscillators. This fact simplifies greatly the analysis of the high-dimensional Josephson-junction arrays considered here. The analysis of the dynamical equation system for type (iii) current distributions, for which at present no experiments are availible, is much more complex and will be discussed elsewhere.[19]

In this paper we discuss the Josephson-junction array model based on the experimentally used array of Fig. 1(a) with type (ii) current distributions. Let I_{ij}^V be the current through a single junction on a vertical branch, V_{ij} the voltage at node (ij), ΔV_j the voltage drop between rows j and $j+1$, I_0 a constant bias current, and I_L the load current. The current-voltage relation for the ideal junction is represented in terms of the Josephson phase differences $\Phi_{ij}^V(t)$ across the vertical and $\Phi_{ij}^H(t)$ across the horizontal junction barriers. The general Josephson relation states that for $I_{ij}^{V,H} < I_c$ there is no voltage drop across the junction with index (ij) and for $I_{ij}^{V,H} > I_c$ the voltage drop is proportional to the time derivative of $\Phi_{ij}^{V,H}$. Hence, for type (i) and type (ii) current distributions it follows that

$$V_{ij} - V_{i+1,j} = 0 \quad \forall i,j, \tag{1}$$

and the application of Kirchhoff's voltage and current laws to the network yields

$$V_{ij} - V_{i,j+1} = \Delta V_j \quad \forall i, \tag{2}$$

$$\sum_i^M I_{ij}^V + I_L = I_0 \quad \forall j. \tag{3}$$

Equation (1) accounts for the fact that there is zero voltage drop between different columns. If $I_{ij}^H < I_c$ and the phase difference semirotates with small amplitude (cf. Sec. III A), Eq. (1) remains valid since semirotations do not induce voltage drops.[8] The identical bus-bar resistors sketched in Fig. 1 are not explicitly taken into account in the analytic description since we deal with general type (ii) current distributions. The ideal RCSJ junction carries the supercurrent i_J, a resistor r, and a capacitor c_J with normal current i_r and i_c, respectively. Hence, $I_{ij}^V = (i_J + i_r + i_c)_{ij}$ $(i = 1, \ldots, M,$ $j = 1, \ldots, N)$ is the total current through a junction in a column with index (ij) and $I_{ij}^H = (i_J)_{ij}$ $(i = 1, \ldots, M-1,$ $j = 1, \ldots, N+1)$ the current through a junction in a horizontal row with node (ij). The supercurrent and the voltage across the junctions are given by the Josephson relations

$$(i_J)_{ij} = I_c \sin \Phi_{ij}^{V,H}, \tag{4}$$

$$\Delta V_j = \frac{\hbar}{2e} \frac{d\Phi_{ij}^V}{dt}, \tag{5}$$

$$0 = \frac{d\Phi_{ij}^H}{dt}, \tag{6}$$

where I_c denotes the critical current of the junctions. Introducing reduced units by measuring the current in units of I_c, voltage in units of $I_c r$, resistance in units of r, capacitance in units of $\hbar/(2eI_c r^2)$, and time in units of $\hbar/(2eI_c r)$, and combining Eqs. (1)–(6) yields the differential equation system

$$\beta \ddot{\Phi}_{ij}^V + \dot{\Phi}_{ij}^V + \frac{1}{M} \sum_k^M \sin \Phi_{kj}^V + \overline{I_L} = \overline{I_0}, \tag{7}$$

$$I_{ij}^H = \sin \Phi_{ij}^H. \tag{8}$$

Here $\beta = 2eI_c r^2 c_J/\hbar$ is a dimensionless measure of the junctions capacitance, overdots indicate derivatives with respect to the time t, and $I_L = I_L/M$ and $I_0 = I_0/M$ are the normalized load and bias currents, respectively.

The macroscopic order parameter phases at each node of the network must be unique. Hence, the 2D network topology requires for the flux flow that, in the absence of external fields, the sum over all junction phase differences, $\Phi_{ij}^{V,H}$, around any closed loop must be an integer multiple of 2π. Therefore, the array equations (7) and (8) must be supplemented by the flux quantization condition

$$\sum_{\text{loop}} \Phi_{ij}^{V,H} = 2\pi k,$$

which for an elementary cell in the network can be written as

$$\Phi_{i,j+1}^H - \Phi_{i,j}^H = 2\pi k_{ij} + \Phi_{i+1,j}^V - \Phi_{i,j}^V. \tag{9}$$

From Eq. (5) it follows that the right-hand side (RHS) of (9) possesses a constant value since the time derivatives of the Φ_{ij}^V are independent of the index i. Consequently, for any given set of Φ_{ij}^V which satisfy (7) the differences of the horizontal phase differences Φ_{ij}^H on the LHS of (9) are fixed. Equation (9) therefore provides current couplings between vertical and horizontal phase differences such that, for any applied input current $I_A = I_0 - \overline{I_L}$, a current distribution within the network which satisfies the Kirchhoff current conservation law at each node of the array, viz.,

$$I_{i,j-1}^V + I_{i-1,j}^H - I_{i,j}^V - I_{i,j}^H = 0, \tag{10}$$

can be computed numerically from the solutions of (7). Differentiating (9) with respect to time leads to Kirchhoff's voltage law for a network unit cell, which therefore is automatically satisfied for all times. By virtue of Eqs. (9) and (10), and since for rectangular arrays of the type considered here the number of horizontal junctions is greater than the number of elementary network cells, the current distribution within the array and the phase differences of the horizontal and vertical junctions, Φ_{ij}^H and Φ_{ij}^V, are not uniquely determined by the input current I_A. Therefore, the current distribution for a given input current depends on inital conditions. For example, for bias currents below the critical current of the array we show in Figs. 2(a) and 2(b) two different supercurrent distributions for an 8×8 array with identical array input current I_A. We used perfect homogeneous column input and output currents and assumed slightly different critical currents of the junctions with a 1σ spread of I_c less than 3%. The results for slightly nonhomogeneous input currents are similar. In both cases the small deviations from perfect homogeneity are sufficient to produce a type (ii) current distribution. This is in full accordance with the fact that in experiments on arrays with bus-bar resistors type (ii) current distributions are the rule. Recently, the dependence of the array dynamics on the initial conditions has also been found experimentally by Doderer and Lachenmann.[20] These authors investigated row switching phenomena in arrays of underdamped junctions using low-temperature scanning electron microscopy. They observed that the spatial distributions of rows of vertical junctions, which are in the voltage state at a fixed bias current, are different for the same sample if the experiments are repeated but the number of rows of oscillating vertical junctions remains the same although their distribution in the array changes. This will be shown in Sec. III to be related to different sequences of row switchings for different initial conditions $\Phi_{ij}^V(0)$. The LTSEM images presented in Ref. 20 are also an impressive experimental proof for the fact that the horizontal junctions do not switch into the voltage state and do not oscillate. Figures 2(c) and 2(d) show a possible evolution of the current distribution of Fig. 2(b) if the bias current is slowly increased up to a magnitude just below the critical current of the array, which is approximately $5I_c$. In Sec. III C we will give an analytical expression for the value of the critical array current. In virtue of Eq. (9) the current distribution remains of type (ii) and the evolution is mainly governed by the increasing currents through the vertical junctions whereas the horizontal currents vary only in a small range. The flux quantization condition and the applied boundary conditions ensure that the horizontal currents remain small, even if the input current I_A is larger than the critical current of the array. On the other hand, the flux quantization constraint also ensures that the horizontal currents do not vanish. The dynamics of the oscillating array states and spatiotemporal patterns is therefore governed by Eq. (7) because the horizontal junctions exhibit only dc Josephson effects. To understand the arrays oscillatory dynamics, the analytical examination of (7) is sufficient. In Sec. III C we test our analytical results by numerically simulating the complete coupled array equation system, Eqs. (7)–(10).

For $M=1$, Eq. (7) reduces to the familiar set of differential equations that describes 1D arrays.[10,12] In the case without an external load all junction phase differences are uncoupled. Hence, the in-phase solution of such 1D systems, where all junctions oscillate coherently, is neutrally stable so that small perturbations or imperfections lead to uncorrelated oscillator phases. In contrast to this, Eq. (7) shows that for $M>1$ even in 2D arrays without an external load, junctions on the vertical branches through the same row are coupled. Furthermore, Eqs. (7)–(10) tell that the in-phase state of the vertical junctions of this type of 2D array is also only neutrally stable because without a shunted load there exists no coupling between junction phase differences Φ_{ij}^V belonging to different rows. This result corresponds to the result obtained in Ref. 9 for the macroscopic order parameter phases of the nodes of the network with perfect homogeneous column input and output currents.

Considering the 2D array shunted by an appropriate load we choose, without loss of generality, a load with capacitance β_L and resistance ρ_L in parallel. In this case the relation between the load current I_L and the total voltage V across the array becomes

$$I_L=\beta_L\dot{V}+\frac{V}{\rho_L}, \tag{11}$$

$$V=\sum_j^N \dot{\Phi}_{ij}^V. \tag{12}$$

Substituting Eqs. (11) and (12) into (7) we obtain the following set of second-order differential equations for the Φ_{ij}^V:

$$\beta\ddot{\Phi}_{ij}^V+\dot{\Phi}_{ij}^V+\frac{\nu}{N}\sum_l^N \dot{\Phi}_{il}^V+\frac{1}{M}\sum_k^M \sin\Phi_{kj}^V-\frac{\mu}{MN}\sum_{k,l}^{M,N} \sin\Phi_{kl}^V=b, \tag{13}$$

where

$$b=\overline{I_0}(1-\mu),\quad \mu=\frac{N\beta_L}{M\beta+N\beta_L},\quad \nu=\frac{N}{M\rho_L}(1-\mu)-\mu. \tag{14}$$

We note that for $\beta_L=0$, i.e., without load capacitance, μ and the global nonlinear coupling term vanish. If in addition $\beta=0$, μ becomes undetermined. In this case the resistively shunted junction (RSJ) model can be used to derive a set of differential equations for the phase differences Φ_{ij}^V which is similar to Eq. (13).

Next we show that Eq. (13) possesses $(M-1)\times N$ constants of motion. Setting

$$\xi_j^{(i)}=\dot{\Phi}_{1j}^V-\dot{\Phi}_{ij}^V,\quad 2\leq i\leq M,\quad 1\leq j\leq N, \tag{15}$$

we obtain from (13) the set of linear differential equations for $(\xi_1^{(i)},\ldots,\xi_N^{(i)})$

$$\beta\dot{\xi}_j^{(i)}=-\xi_j^{(i)}-\frac{\nu}{N}\sum_l \xi_l^{(i)}. \tag{16}$$

The matrix on the RHS of (16) has an $(N-1)$-fold eigenvalue -1 and a single eigenvalue $-(\nu/N+N)$. Therefore $\xi_j^{(i)}\to 0$ for $t\to\infty$ and there exists an attracting invariant subspace, given by

$$\xi_j^{(i)}=0,\quad 2\leq i\leq M,\quad 1\leq j\leq N. \tag{17}$$

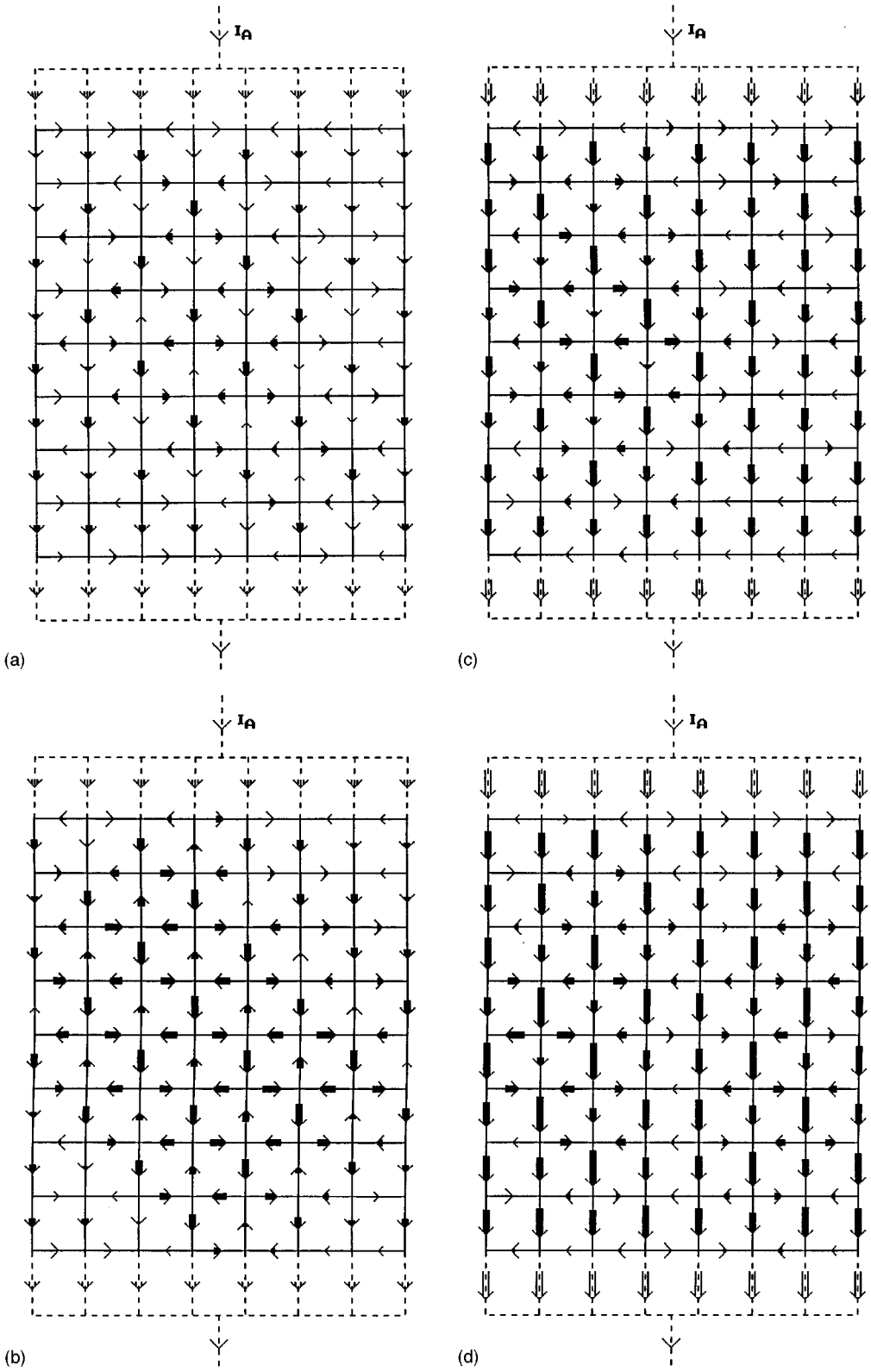

FIG. 2. Current distributions within a 8×8 network of Josephson junctions for different input current I_A and slightly different critical currents of the junctions, $(I_c)_{ij}^{V,H}=I_c(1\pm\epsilon_{ij}^{V,H})$, $\epsilon\ll1$, for arrays with bus-bar resistors. The junctions themselves are not shown [see Fig. 1(a)]. The length of the arrows is proportional to the currents $I_{ij}^{V,H}$ (a full cell length corresponds to a current of I_c; small arrows indicate $|I_{ij}^{V,H}|<10^{-2}I_c$). (a),(b) $I_A=1I_c$, perfect homogeneous column inputs and outputs with 1σ spread of the critical currents smaller than 3%. In virtue of different initial conditions in (a) and (b) represented here, e.g., by different I_{i1}^{H}, the supercurrent distributions in the array differ significantly. (c),(d) Evolution of current distribution (b) with increasing array current I_A: (c) $I_A=3I_c$, (d) $I_A=4.5I_c$. In (d) I_A is slightly below the array's critical current of approximately $5I_c$. By virtue of flux quantization the horizontal currents I_{ij}^{H} remain less than I_c.

For arbitrary initial conditions, this invariant subspace corresponds to the constraints of Eq. (1). It is therefore possible to derive a reduced set of differential equations directly from (7) and (11). With (1) and (2) it follows from (5) that

$$\dot{\Phi}_{ij}^{V}=\dot{\Phi}_{1j}^{V} \tag{18}$$

$\forall i$ and any given j. The time evolution of the individual junction phases can therefore be represented in the form

$$\Phi_{ij}^{V}(t)=\phi_j(t)+\Psi_{ij}, \tag{19}$$

where the Ψ_{ij} are constants of motion, i.e., time independent frozen phase slips and $\phi_j(0)=0$, without loss of generality. The $\Psi_{ij}=\Phi_{ij}^{V}(0)$ define the initial conditions imposed on the 2D array by a given input pattern and $\dot{\Phi}_{ij}^{V}(0)=\dot{\phi}_j(0)$ satisfy (12). The same procedure used to derive Eq. (13) from (7) yields then for ϕ_j the equation system

$$\beta\ddot{\phi}_j+\frac{\beta_L}{M}\sum_k \ddot{\phi}_k+\frac{1}{M\rho_l}\sum_k \dot{\phi}_k+\dot{\phi}_j+\frac{1}{M}\sum_i \sin(\phi_j+\Psi_{ij}) =\overline{I_0}. \tag{20}$$

To rewrite (20) in a more convenient form we introduce new coupling parameters a_j and phase shifts δ_j $(1\leqslant j\leqslant N)$. By setting $(1/M)\Sigma_i\sin(\phi_j+\Psi_{ij})=a_j\sin(\phi_j+\delta_j)$ the a_j and δ_j are related to the Ψ_{ij} by

$$\frac{1}{M}\sum_i \cos\Psi_{ij}=a_j\cos\delta_j, \quad \frac{1}{M}\sum_i \sin\Psi_{ij}=a_j\sin\delta_j, \tag{21}$$

and

$$0\leqslant a_j^2=\frac{1}{M^2}\sum_{k,l} \cos(\Psi_{kj}-\Psi_{lj}) =\frac{1}{M}+\frac{2}{M^2}\sum_{k<l} \cos(\Psi_{kj}-\Psi_{lj})\leqslant 1, \tag{22}$$

with

$$\sum_i \sin(\Psi_{ij}-\delta_j)=0. \tag{23}$$

The differential equation system (20) for the phases ϕ_j takes now the form

$$\beta\ddot{\phi}_j+\dot{\phi}_j+\frac{\nu}{N}\sum_l \dot{\phi}_l+a_j\sin(\phi_j+\delta_j)-\frac{\mu}{N}\sum_l a_l\sin(\phi_l+\delta_l) =b, \tag{24}$$

which, with the translation $\phi_j\rightarrow\phi_j-\delta_j$, simplifies to

$$\beta\ddot{\phi}_j+\dot{\phi}_j+a_j\sin\phi_j+\frac{\nu}{N}\sum_l \dot{\phi}_l-\frac{\mu}{N}\sum_l a_l\sin\phi_l=b, \tag{25}$$

where b, ν, and μ are defined by Eq. (14).

In virtue of (19) and (21) the $(N\times M)$-dimensional uniform 2D array equation system (13) has been transformed into a one-dimensional, nonuniform, and nonlinear chain equation system (25) for N phase oscillators and there is a one-to-one correspondence between the solutions of (13) and (25). Equation (25) can be interpreted as a series array of nonidentical, nonuniformly, and globally coupled Josephson junctions with long-range interaction and different values of the ''reduced critical currents'' a_j for different j. Alternatively, Eq. (25) can be viewed as the equation system for a nonlinear chain of damped physical pendulums or rotating disks with nonuniform mass distribution coupled globally to each other and driven by a common torque b. This visualization of (25) is helpful in an intuitive interpretation of our results.

We observe that the 2D array, Eq. (13), is invariant under any permutation of the indices within the rows and under permutations of the rows themselves and so possesses a wreath product symmetry.[23] Since the couplings a_j in Eq. (25) are determined by the conditions (21), i.e., by the initial conditions Ψ_{ij}, this symmetry reduces to a combined parameter symmetry where the a_j and the ϕ_j can be permuted simultaneously. If the Ψ_{ij} are equally spaced around the unit circle for a given j, the corresponding a_j vanishes.

III. DYNAMIC PATTERNS IN JOSEPHSON ARRAYS

In this and the subsequent section we discuss the macroscopic pattern dynamics described by Eqs. (13) and (25) analytically, compare the theoretical predictions with recent experimental results, and discuss their physical implications for phase coherence, pattern recognition, and 3D high-temperature superconductors. We begin in Sec. III A with a brief description of the types of motion a single Josephson phase oscillator [physical pendulum] can perform inside the chain (25) and then consider in Sec. III B the coupled system in the theoretical and experimental context. In Sec. III C we discuss numerical simulations and in Sec. III D we analyze the array's phase space dynamics.

A. Dynamics of a single oscillator

Equation (25), to which the 2D system (13) has been reduced, describes a one-dimensional chain of nonuniformly and globally coupled, nonlinear and nonidentical phase oscillators. We consider first an isolated, uncoupled oscillator. Its time evolution is governed by

$$\beta\ddot{\phi}_j+\dot{\phi}_j+a_j\sin\phi_j=b. \tag{26}$$

Since one of our goals is to elucidate the dependence of the oscillation frequencies and phases in Eq. (25) on the parameters a_j, we do not perform a time rescaling which would yield $a_j=1$, because for the coupled system such a transformation is not possible and the different values of $|a_j|\leqslant 1$ influence the degree of nonlinearities. We discuss briefly the properties of Eq. (26) in the context of Eq. (25).

For $b<|a_j|$, Eq. (26) has a stable rest point $\phi_j^{+}=\sin^{-1}(b/a_j)$. If in the case of the physical pendulum the torque b is slowly increased from $b=0$, the pendulum moves away from the downward vertical to the new stable equilibrium angle ϕ_j^{+}. When $b>|a_j|$, Eq. (26) has a stable 2π periodic running, physically whirling, solution given by a function $\phi_j=\phi_j^{*}(t)$ with $\phi_j^{*}(t+T)=\phi_j^{*}(t)+2\pi$ where T is the rotation period. Interpreting (26) as an ac Josephson

junction, the time-averaged angular velocity $v=\langle \dot{\phi}_j^* \rangle$ corresponds to the junction voltage V, b to the bias current I_0, and a_j to an (in general) reduced ''effective'' critical current. For nonwhirling periodic solutions, in the nonlinear context known as semirotors (cf. below), v vanishes.[8] If the junction is underdamped, i.e., if β is sufficiently large, then, due to inertia, slowly decreasing the bias current b from the whirling value induces a hysteresis loop in the current-voltage curve. For large β and small a_j it can therefore happen that the whirling persists down to $b=0$. If, on the other hand, β is small (i.e., $\beta<1$), the junction will retrace its original b-v or I-V curve.

For the interpretation of our numerical simulations of Eq. (13) and for comparison with experiments and technical applications, the averaged frequency ω of the running solution $\phi_j^*(t)$ of Eq. (26) must be determined as a function of the parameters β, a_j, and b. To this end we apply the method of harmonic balance by setting

$$\phi_j^* = \phi_0 + \omega t + A\cos(\omega t) \tag{27}$$

and neglecting higher-harmonic terms. Substituting this ansatz into Eq. (26) we use the expansion

$$\sin(\phi_j^*) \simeq J_0 \sin(\omega t + \phi_0) + J_1 \cos(\phi_0), \tag{28}$$

where $J_n = J_n(A)$ is the nth-order Bessel function of argument A. By separately balancing terms which are constant, proportional to $\cos(\omega t)$, and proportional to $\sin(\omega t)$ we find three algebraic equations for ϕ_0, ω, and A:

$$\omega + a_j J_1 \cos(\phi_0) = b, \tag{29}$$

$$-A\omega + a_j J_0 \cos(\phi_0) = 0, \tag{30}$$

$$-A\beta\omega^2 + a_j J_0 \sin(\phi_0) = 0. \tag{31}$$

From this the equation for the frequency ω follows:

$$(b-\omega)\sqrt{\omega^2 + \frac{1}{\beta^2}} = \frac{a_j}{\beta} J_1. \tag{32}$$

Since $|a_j| \leqslant 1$ and $|J_1| \ll 1$, for large enough β, i.e., $\beta > 1$, the averaged frequency ω is nearly identical for all oscillators (and equal to b) irrespective of the value of a_j. Thus, in the weakly coupled system (25) frequency synchronization will occur. If β is small, especially if $\beta < 1$, we expect that for low values of b the coupled system shows quasiperiodic or aperiodic behavior because several different frequencies can coexist in the chain.

In the limit $\beta = \beta_L = 0$, but also for small β, the frequency of a single oscillator can be determined using the fact that ϕ_j^* is 2π periodic and is given by

$$\omega = c\sqrt{1 - \frac{a_j^2}{c^2}}, \tag{33}$$

where for the coupled system of RSJ's

$$c = \overline{I_0}(1-\chi) \quad \text{and} \quad \chi = \frac{N}{N + M\rho_l} \tag{34}$$

correspond to the torque b and the coupling μ in Eq. (14), respectively. Depending on the value of a_j, for small bias current the frequencies of the individual oscillators may differ significantly so that frequency synchronization is not ensured.

With regard to the coupled system (25) considered in the next section, an additional periodic solution of Eq. (26) which, although unstable in the uncoupled system, is known to exist.[10,22] This nonwhirling periodic solution is called semirotor or libration since it is given by some function ϕ_j^{**} where $\phi_j^{**}(t+T) = \phi_j^{**}(t)$. The motion of a semirotor corresponds to that of a pendulum in the small-angle approximation. If such a semirotor exists and is stable in the coupled system (25) its approximated averaged frequency is also given by (32) or (33), respectively.

B. Dynamics of 2D arrays

We are now prepared to discuss the dynamical patterns which are generated in the 2D array (13) or (25) in response to variable bias currents, coupling strength, and initial conditions.

The basic dynamical patterns to be expected arise (i) from the set of nontrivial fixed points of (25), (ii) from the bifurcation of semirotations from the latter, and (iii) from the bifurcations of whirling rotational states from fixed points or semirotations which lose their stability when the bias current, acting as a bifurcation parameter, goes through critical values given by the a_j in Eq. (25). Since, in general, according to Eq. (32) or (33) with each bifurcation into an oscillatory state (semirotating or whirling) a new frequency appears with which groups of junctions oscillate, we discuss in detail the mechanisms responsible for frequency synchronization. The spatial distribution of the oscillatory patterns is related to the wreath product symmetry of Eq. (13) and, therfore, to the combined parameter symmetry of Eq. (25), mentioned in Sec. II. This symmetry of the network equations allows the simultaneous coexistence of fixed points, semirotors, and whirling states with different frequencies in different array compartments, with the phases in general distributed incoherently.

The $N \times M$ dimensional equilibrium point of Eq. (13) is given by

$$\sum_k^M \sin\Phi_{kj}^V = I_0 \quad \forall j. \tag{35}$$

Hence, in virtue of Eq. (19), the stable equilibria form a $[N\times(M-1)]$-dimensional manifold in the space of the Φ_{ij}^V which is given by $\Phi_{ij}^V = \Psi_{ij} - \eta_j$, where the η_j satisfy

$$\sum_k^M \sin(\Psi_{kj} - \eta_j) = I_0 \quad \forall j, \tag{36}$$

with $\eta_j \in [-\pi, \pi]$ and $\eta_j = \delta_j$ for $I_0 = 0$. In contrast with 1D arrays, even for $I_0 = 0$, the oscillators must not reach the trivial equilibrium ($\Phi_{ij}^V = 0$) because the frozen phase slips Ψ_{ij}, which are constants of motion, are in general different. If we associate each phase difference Φ_{ij}^V with a point on the unit circle, then, in the equilibrium position the phases of the junctions are distributed nonuniformly on this circle. This is allowed because in the 2D array only the sum of all vertical currents has to satisfy Eq. (3). For any fixed I_0 the values of

the equilibrium manifold depend on the initial conditions only and not on system parameters. This fact follows already from Eq. (7) because even without an external load the coupling is identical for all junction phases Φ_{ij}^V within the same row.

To discuss the oscillatory patterns of the 2D array analytically we use Eq. (25) rather than Eq. (13). The stable equilibrium point of Eq. (25) is given by the isolated fixed points $\phi_j^{++}=\sin^{-1}(I_0/a_j)$ with $j=1,\ldots,N$. For $I_0>|a_j|$ they lose their stability so that the onset of oscillations in the coupled system, Eq. (13) [Eq. (25)], is governed by the smallest $|a_j|$. We order the individual critical currents or row couplings a_j by taking their absolute values and interchanging their indices such that

$$|a_1|\leqslant|a_2|\leqslant|a_3|\leqslant\cdots\leqslant|a_N|. \tag{37}$$

For $\overline{I_0}>|a_1|$ the stable fixed point ϕ_j^{++} of (25) loses its stability and the system begins to oscillate. We shall show below that, in contrast with general globally coupled homogeneous systems,[24–26] certain groups of junctions in the 2D array (13) exhibit now different bifurcation scenarios and the onset of qualitatively different oscillations occurs in spatially localized compartments, which according to (25), in the case of absolutely identical junctions, consist of the array's rows themselves. Thus the geometrically uniform 2D array behaves dynamically nonuniform.

Indeed, if the normalized bias current $\overline{I_0}$, considered as a bifurcation parameter, approaches $|a_1|$ from below, then, according to (25) and Sec. III A the phase oscillators in the row belonging to a_1, i.e., in the first compartment, start to whirl simultaneously with the same frequency but phase incoherently. This whirling generates the first voltage step at $|a_1|$ in the I-V characteristics because in the expression for the voltage $V=\langle\Sigma_{k=1}^N\dot{\Phi}_{ik}^V\rangle$ (where the brackets denote time averaging) $\dot{\Phi}_{ik}^V=\dot{\phi}_k$ is different from zero only for the k belonging to a_1 while $V=0$ for fixed points and semirotors. If there would be no coupling between compartments constituted by the array's rows belonging to a_j, $j\geqslant1$, then, as the increasing I_0 passes through the sequence of critical values (37), the oscillator phases in the succcessive rows start immediately to whirl, producing a staircase succession of voltage steps at $\overline{I_0}=|a_j|$, $j=1,\ldots,N$, until the I-V characteristics become linear for $I_0>|a_N|$ when all junction phases Φ_{ij}^V of the network oscillate with the same frequency but phase incoherently and the compartments merge into a single block. Since, however, the rows are coupled, the whirling of phase oscillators in the first row (a_1) generated at $\overline{I_0}=|a_1|$ leaves the other rows staying in their fixed points as long as $I_0<|a_2|$. If $\overline{I_0}$ reaches the bifurcation point $|a_2|$, the phases in row 2 start to oscillate as semirotors. Since $\langle\dot{\Phi}_{ij}^V\rangle=0$ for fixed points and semirotors these do not contribute to V. If $\overline{I_0}$ increases further, the semirotating oscillators of row 2 bifurcate into fully whirling states at some $I_0=a_2^*>|a_2|$ because the damping term $\nu/N\Sigma_l\dot{\phi}_l$ in Eq. (25) is now counterbalanced by the sufficiently high value of I_0. In this way, at successive values $\overline{I_0}=a_j^*>|a_j|$, $j\geqslant2$, the rows in the coupled system start to whirl, giving rise to steps in the I-V characteristics at values a_j^* rather than a_j whose magnitude depends on the coupling strengths μ, ν and [by virtue of Eq. (25)] sensitively on the values and signs of the remaining set of the a_j [cf. Fig. 3(a)]. However, the succession of fully whirling oscillation onsets at a_j^* and voltage steps follows that of Eq. (37). The frequency ω of the incoherent phase oscillations in a single row compartment is given by Eq. (32) or (33), depending on the value of β. ω is a function of the bias current I_0 and the load parameters ρ_L and β_L, while the incoherence of the oscillations is due to the, in general, nonuniform distribution of the phase slips Ψ_{ij} on which the a_j depend. The height of the steps in the I-V characteristics depends on the initial frequency of the whirling oscillations. Since the fixed point ϕ_j^{++} loses its stability at $I_0=M|a_j|$ the staircase steps begin for $|a_j|\ll1$ at values of I_0 less than the critical current (I_c) of a single junction. This explains, at a dynamical level, the ''row switching'' phenomena [cf. Fig. 3(b)] found recently in experiments.[13,16,17] From Eq. (32) it follows that for sufficiently large β all whirling oscillators will synchronize their frequencies (cf.

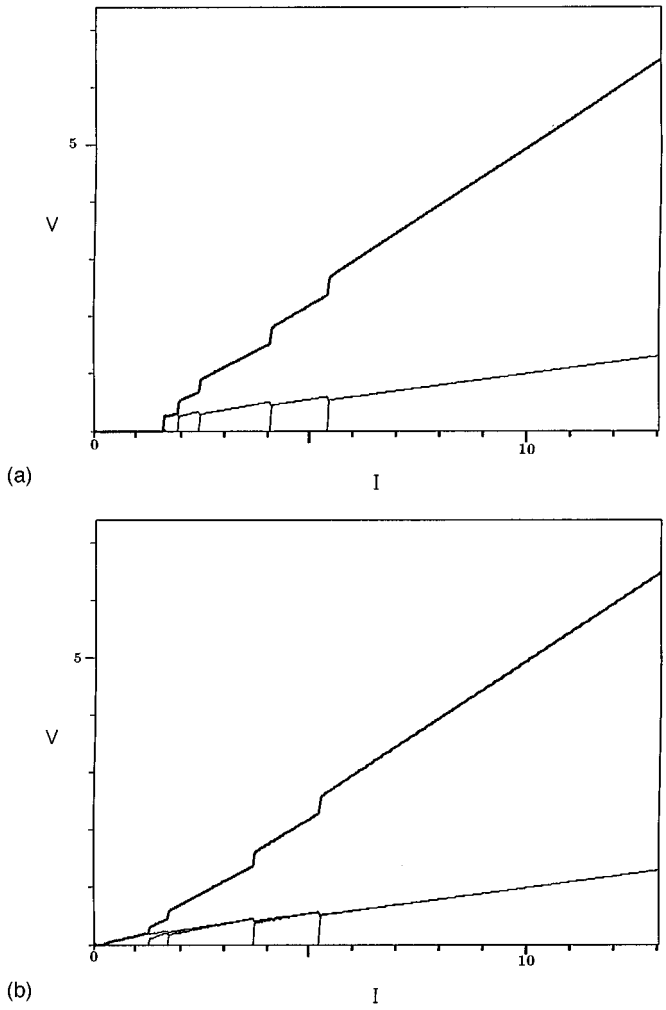

FIG. 3. (a) Simulation of the I-V characteristics (thick) of Eq. (13) taking account of Eqs. (9) and (10) for a 5×5 array with $\beta=10$ (top). The thin curves (bottom) describe the onset of oscillations in successive rows $j=3,4,5,1,2$. Adding these curves yields the curve above. (b) Row switching (in row $j=3$) for the same array with $\beta=5$. The frequencies do not synchronize between rows 3,4 (double curves).

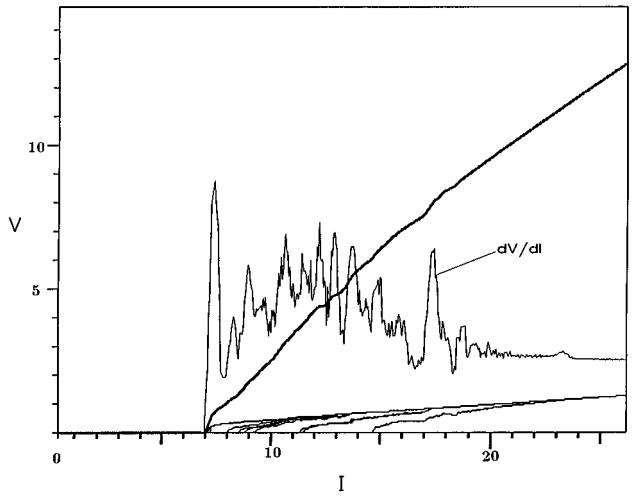

FIG. 4. Simulated I-V characteristics for a 10×10 array with the experimental value $\beta=0.7$ for overdamped junctions and large blocking capacitance, and differential resistance $(dV/dI)(I)$. The sharp peaks in the $(dV/dI)(I)$ resistance curve are generated by the onset of whirling oscillations and by partial frequency synchronization. Distinct array rows self-synchronize to compartments with subharmonic frequencies. The first step takes place at $I=7I_c$.

Fig. 3) completely, although not their phases, even within the transition interval, whereas for $\beta<1$ frequency entrainment is not ensured (cf. Fig. 4).

For sufficiently high values of $\overline{I_0}>a_N^*$, i.e., beyond the transition interval $[|a_1|,a_N^*]$, frequency entrainment occurs according to (32) or (33), the compartments merge into a single oscillating block, and the current-voltage characteristics of the 2D array become linear with the common frequency of the junctions increasing with $\overline{I_0}$. At the same time the dynamics of the 2D network tends towards a continuous family of incoherent phase oscillations with equal frequency. The phase slips between the oscillator phases within one row are given by the Ψ_{ij} of Eq. (19) and the phase shifts δ_j between different rows converge to constant values (cf. Fig. 8), implying in this case a totally phase-locked spatially incoherent limiting state depending on the input pattern defined by the initial condition imposed on Eq. (13). This family of incoherent phase-locked oscillations forms the attractors of the Josephson network dynamics.

C. Simulation of I-V characteristics

We have tested our analytical predictions by numerically integrating Eq. (13) taking account of Eqs. (9) and (10). We simulated square arrays with $5\leqslant M=N\leqslant10$. Impedance matching, i.e., $\rho_L=1$, and large blocking capacitance, i.e., $\beta_L=10\beta$, ensured sufficiently large global coupling strengths μ and ν. According to the discussion in Sec. II we observed in all simulations that the phase differences of the horizontal junctions do not whirl ($I_{ij}^H<I_c$), and that they do not influence the oscillatory states and spatiotemporal patterns the arrays exhibit. The phase differences Φ_{ij}^H of the horizontal junctions possibly semirotate with low amplitude, but according to Sec. III A these semirotations are not accompanied by voltage drops in the horizontal direction. Above the bifurcation point the current distribution in the array is, according to Eqs. (3) and (8), similar to that in Fig. 2(d) and for increasing I_A determined by the increasing vertical currents. The current-voltage curves are generated by slowly increasing or decreasing the bias current I_0 and observing the long-time average voltage $V=\langle 1/M\Sigma_{k,l}^{M,N}\dot{\Phi}_{kl}^V\rangle$. The bias current $I=I_0$ is measured in units of I_c, and V in units of I_cr. The thick lines in the I-V characteristics describe the characteristics of the whole circuit, the thin curves the onset of whirling solutions in particular rows. For a given I_0 the initial conditions for the Φ_{ij}^V are chosen by random such that Eqs. (9), (10), and (13) are satisfied. From Eq. (21) it follows that for randomly chosen initial values Ψ_{ij} equally partitioned in the interval $[-\pi/2,\pi/2]$ the mean value of the reduced critical current $|a_j|$ converges rapidly to $2/\pi=0.63$ for increasing M. For $M=10$ this implies that in a 10×10 array the measured critical current of the array is 63% of the value 10 I_c where I_c is the critical current of a single tunneling contact. This theoretical prediction agrees with the critical current measured by Lachenmann *et al.*[16] Our examination of the possible inhomogeneous current distributions (cf. Sec. II) indicates that for values of the vertical currents I_{ij}^V that correspond to such initial conditions the occurrence of eddy currents in the network unit cells is extremly unlikely. The accordance with the experimental measurement may be explained with the tendency of the current distribution to avoid eddy currents for array currents I_A that are comparable with the critical current of the array because they are energetically unfavorable.[27] This argument can also explain why in experiments the I-V characteristics are reproducible in some details within measurement accuracy. If there are no perturbations by moving vortices, the couplings a_j and therefore the sequence of bifurcations (37) are strongly influenced by perturbation matrices which are given by the deviations of the individual junction parameters I_c, r, and c_J from the assumed equality of all junctions which are produced by imperfections (cf. Sec. II). Since these imperfections are a natural result of the fabrication process, the perturbation matrices are fixed for a given array and do not change if the experiments are repeated. To reproduce this experimental situation, the initial conditions for the Ψ_{ij} in all simulations are chosen from the interval $[-\pi/2,\pi/2]$ and $\dot{\Phi}_{ij}^V(0)=0$ and, if perturbations are included in the simulations, it is assumed that they have the form of time-constant perturbation matrices.

Figure 3(a) shows the I-V curve of a 5×5 array with $\beta=10$ and $\beta_L=100$. Using Eq. (21) the set of couplings is given by $(a_1,\ldots,a_5)=(0.63,0.81,0.34,0.41,0.53)$. The first bifurcation point occurs exactly at $I=Ma_3=1.7$, as expected from our calculation of the fixed points of Eq. (25). All other bifurcations into the whirling state occur at points $I=a_j^*>|a_j|$. The staircase with the N predicted steps is easily recognized, because successive rows switch into the voltage state (whirling state) according to the sequence $j=(3,4,5,1,2)$. In addition, although the a_j are different, β and the global coupling parameters ν and μ are large enough to enforce frequency entrainment already within the transition interval. The small decreasing steps in the I-V characteristics of the individual rows are due to this entrainment mechanism because for large blocking capacitance β_L and impedance matching the value of the coupling parameter ν becomes negative.

The I-V curve for the same array configuration but with $\beta=5$ is shown in Fig. 3(b). The individual row couplings are given by the set $a_j=(0.46,0.57,0.04,0.25,0.2)$. The first bifurcation point appears at $I=Ma_3=0.2$ and the row switching phenomena is obvious. However, in contrast with Fig. 3(a), there is no frequency entrainment within the transition interval. Only for values of I beyond the last bifurcation point a_2^* do the frequencies synchronize. From Eq. (32) such behavior is to be expected because $a_3=0.04$ differs significantly from the absolute values of the other a_j.

Next we consider values of $\beta<1$. Figure 4 shows the I-V curve of a 10×10 array with $\beta=0.7$ together with the differential resistance $(dV/dI)(I)$. For $a_j=(0.7,0.72,0.87,0.77,0.75,0.79,0.71,0.76,0.85,0.91)$ the initial bifurcation point is given by $I=7.0$. In the I-V curve only the first step of the staircase is properly resolved because within the transition interval the different frequencies of the bifurcating rows do not synchronize with the frequency of their predecessors. In accordance with our theoretical considerations, bias currents I much larger than MI_c will be needed to achieve frequency synchronization. The $(dV/dI)(I)$ resistance curve shows sharp peaks at the onset of whirling oscillations in succeeding rows and additional peaks when frequency synchronization occurs. Moreover, by inspection of the I-V characteristics of the individual rows for $12.5<I<13.7$ and $15.8<I<17.1$, regions in which distinct rows of oscillators self-synchronize to subharmonic frequencies can be observed and the magnitude of these subharmonic frequencies is half of that of the frequency of the remaining oscillators. These array states appear to be stable for intervals of I which are larger than I_c and, therefore, have the consequence that the value of the bias current for which the I-V characteristics becomes linear is shifted towards $I\simeq25$. Figure 4 reproduces the experimentally measured curve.[20]

If small parameter spreads and noise are included in the numerical simulations of the array model (9), (10), and (13), stochastic switchings between different array states take place near the voltage steps and hysteresis loops of different orientations occur within the transition interval. These results are also in close agreement with recent experimental data.[21] The junction parameters I_c, r, and c_J are chosen to have a 1σ spread of less than 3% and to the bias current I white noise with magnitude less than 1% is added. Figure 5 shows the I-V curve of a 5×5 array with $\beta=0.7$ and $a_j=(0.33,0.09,0.44,0.47,0.1)$. Within the transition interval on and off switchings of different rows occur. To examine the stochastic nature of these switchings, in Fig. 6, V is plotted versus time at one distinct value of the bias current. For $I=4$ and $\beta=10$ the 10×10 array indeed exhibits irregular jumps between different array states. Moreover, by careful inspection five distinct states can be observed where different compartments are in the voltage state. The lifetimes of the different states depend on the magnitude of the perturbations and on the value of I. Near the voltage jumps they are typically some ms, but in the intermediate regions they can also take values of some minutes or even days.

From Eq. (21) it follows that for equally distributed initial conditions Ψ_{ij} for a given j the corresponding coupling a_j and the nonlinear term pertaining to it in Eq. (25) vanish.

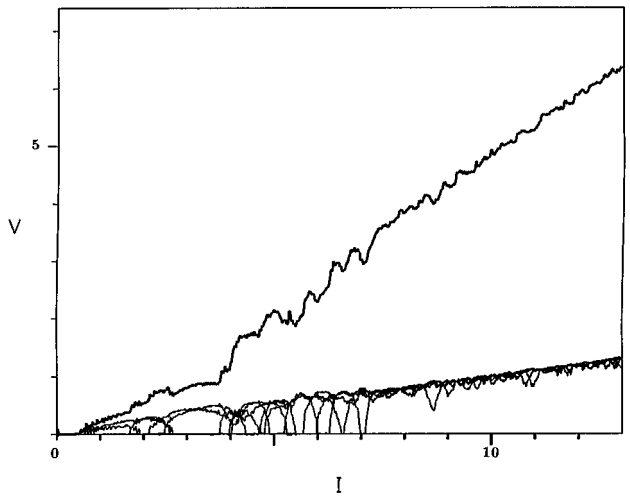

FIG. 5. Simulation of the I-V curve of a 5×5 array with $\beta=0.7$ including small parameter spreads and current fluctuations. Within a transition interval the system jumps between different array states. Several array rows switch on and off with increasing bias current.

Hence, if in the case of small a_j β is chosen sufficiently large, the I-V characteristics exhibit a hysteresis loop whose smooth return branch to low I passes alternatively above and below the staircase and reaches the V axis at a positive value of the voltage, implying that collective whirling persists down to vanishing current. Figure 7 shows a hysteresis loop in one compartment of a perturbed 10×10 system. The return branch of the I-V characteristics crosses the V axis at a small but positive value so that in the corresponding compartment whirling continues some time after the bias current is switched off. In virtue of the perturbations, hysteresis loops of different orientation are observable.

D. Phase space dynamics

Within the transition interval defined by the range of values of $\overline{I_0}$ between $|a_1|$ and the last step a_N^* of the staircase, the nonwhirling semirotating oscillators of the Josephson array are driven by the whirling ones and vice versa. Consequently, depending on the values of β and the coupling

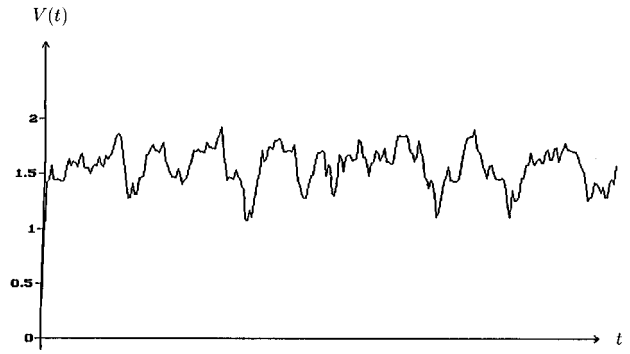

FIG. 6. Long-time averaged voltage V vs time t near a voltage step for the perturbed 2D array. For $I=4$ and $\beta=10$ the 10×10 array exhibits irregular jumpings between different energy levels. By careful inspection five distinct energy levels can be observed. The lifetimes of the different array states are typically some ms.

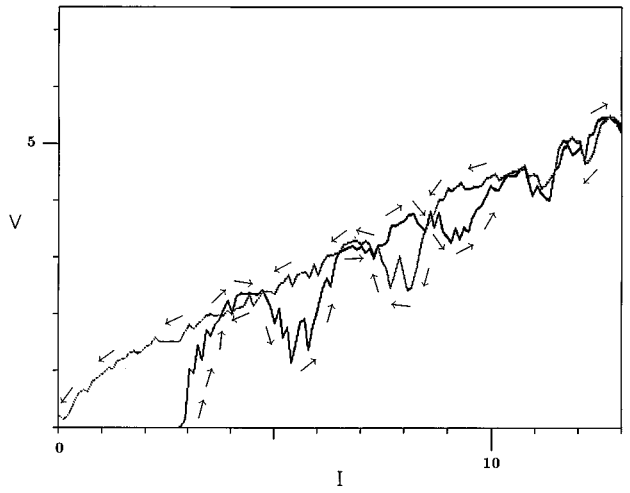

FIG. 7. Hysteresis in the I-V characteristics of a single compartment in the perturbed 2D array. The return branch (dotted line) crosses the ascending branch (thick line) at different values of I, implying a number of hysteresis loops with opposite direction. Rotations persist down to vanishing bias current.

strengths a_j, there exist simultaneously several different frequencies and whirling solutions, semirotors, and fixed points in different compartments of the array. Since the latter are coupled, so are the different nonlinear oscillatory modes and, therefore, aperiodic (chaotic) mixed states of whirling and semirotating as well as quasiperiodic solutions coexist in the 2D Josephson array in different spatially localized domains.

These intrinsic interactions of different compartments and the complicated sequences of phase states the array passes through in generating staircase current-voltage characteristics are revealed by numerically integrating (13) and plotting bifurcation diagrams and snapshots of the phase space dynamics of the oscillators. Figures 8(a) and 8(b) show how successive bifurcations of fixed points, semirotations, and whirlings lead to entangled internal ''crisis scenarios'' in a 10×10 array in virtue of the interaction of different dynamical states in different array compartments. Out of these a new order emerges for increasing I when all compartments whirl and the array enters a frequency-synchronized and phase-locked state. In both figures, for each dc bias level, the values of the phases Φ_{1j} (modulo 2π) of the junctions in the first column of the array are plotted as a function of the slowly increasing bias current. Region (I) in Fig. 8(a) ($\beta=0.7$) and Fig. 8(b) ($\beta=10$) shows the evolution, with increasing I, of the fixed points of Eq. (13) for the same given input pattern. In regions (II) and (III) the initial phases of the junctions for each of 10^4 successive cycles are plotted when the leading compartment in the column, i.e., that which first starts to whirl (a_1: I axis), begins one cycle. The dynamics within the transition interval (II) depends strongly on the value of β. In region (IIa), defined by $M|a_1|<I<M$, the bifurcations from the $N\times M$ dimensional fixed point predicted analytically in Sec. III B take place and fixed points, semirotors and whirling solutions coexist in different rows. Region (IIb), defined by $M<I<Ma_N^*$, exhibits only semirotations and whirlings. Ascending or descending thick curves in region (II) of Fig. 8(b) indicate periodic semirotations (librations), whereas the

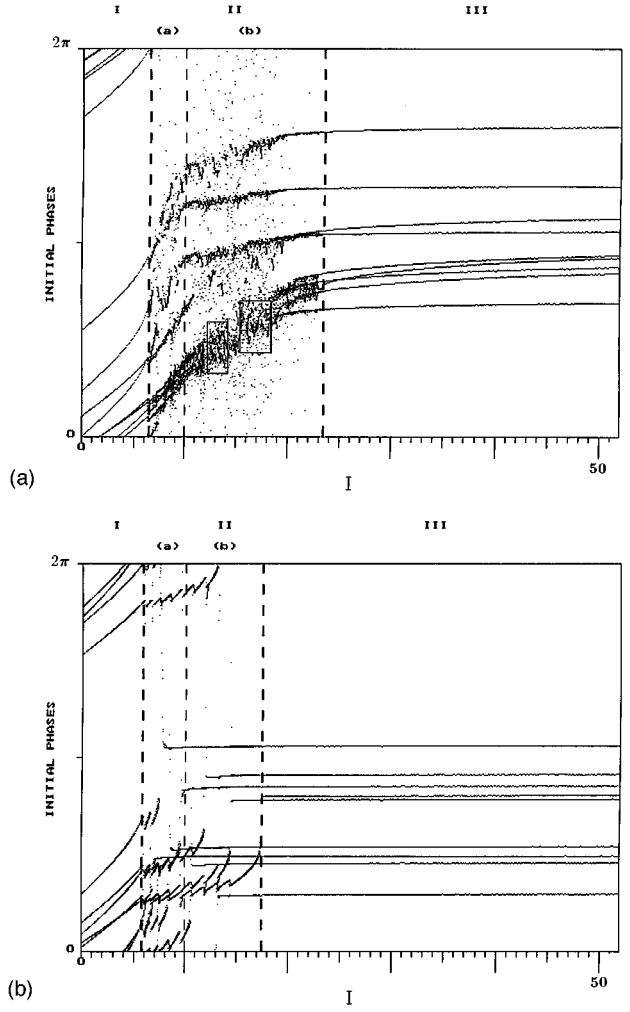

FIG. 8. Initial phases (modulo 2π) as a function of the dc bias current I for a 10×10 array with (a) $\beta=0.7$ and (b) $\beta=10$. In region (I) the fixed points of Eq. (13) evolve along slightly bent lines. In regions (II) and (III), for each dc bias level, the values of the phases in the first column at the beginning of the whirling cycle of the first fully whirling row (a_1) are plotted for 10^4 successive cycles. The windows in region (II) of (a) indicate intervals of I where self-synchronization of particular compartments to subharmonic frequencies occurs (cf. Fig. 4). The thick lines in region (II) of (b) represent semirotations.

semirotors in region (IIa) of Fig. 8(a) are aperiodic and only their tonguelike ''ghosts'' are visible. In region (IIb) of Fig. 8(a) it is not possible to distinguish between aperiodic semirotations and mixed states of semirotation and whirling (cf. Fig. 9). The horizontal curves in regions (IIb) and (III) represent pure whirling states and indicate phase locking of particular compartments with the leading compartment. In Fig. 8(a) each onset of a whirling state in a particular compartment can be directly compared with the corresponding one in Fig. 4 which generates a voltage step in the I-V charcteristics of Fig. 4. The spontaneous reordering of the phases at the beginning of region (III) is due to frequency synchronization in accordance with our theoretical considerations in Sec. III A. For $\beta<1$ region (IIb) is larger than for $\beta>1$ and one can expect that for $\beta\gg1$ region (IIb) disappears. However, according to Eqs. (23) and (37) in all cases the phase shifts

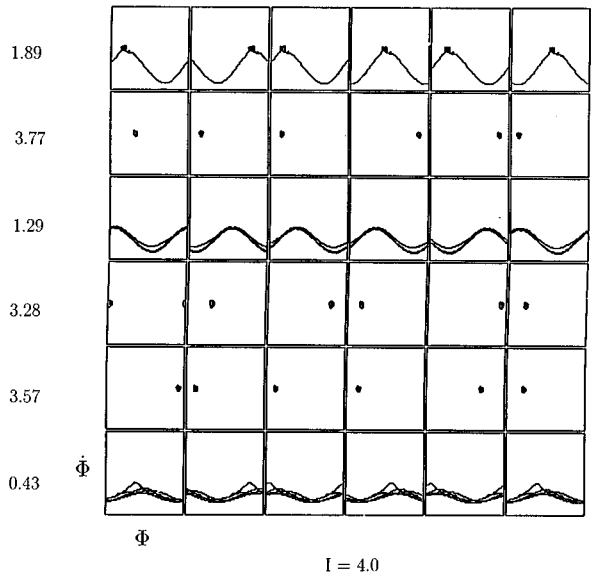

FIG. 9. Phase diagrams of oscillations in a 6×6 array with $\beta=0.7$ for bias current $I=4$. Each box represents the phase space $(\Phi,\dot{\Phi})$ of a distinct oscillator in one of the six row compartments. The numbers on the left are the values of the row parameters $M|a_j|$. The phase space of a single junction is a cylinder. Large dots (resolved in Figs. 10 and 11) represent semirotations on the cylinder, the curves whirlings around the cylinder.

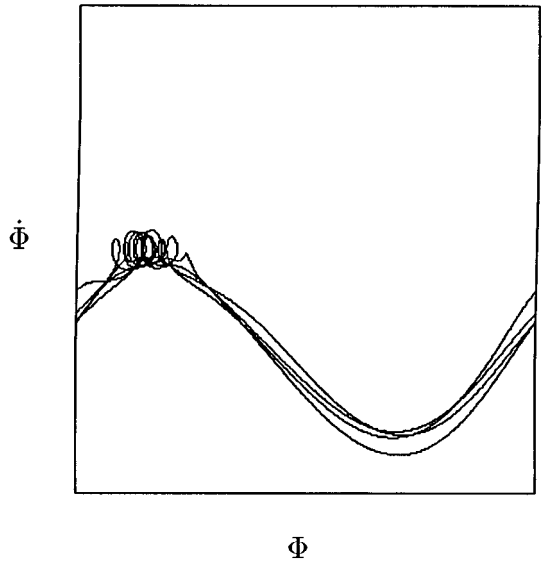

FIG. 10. Spatially resolved phase space diagram of the single junction $i=1$, $j=1$ in Fig. 9 in an aperiodic mixed state of whirling and semirotation within the transition interval.

δ_j between different rows converge to constant values, implying an incoherent but completely phase-locked state in region (III), i.e., on the linear branch of the I-V characteristics in Figs. 3 and 4. In the two small windows of Fig. 8(a) ''aperiodic subharmonics'' are present which imply that four compartments self-synchronize to an averaged frequency with half of the magnitude of the frequency of the leading compartment. These are the subharmonics observed in Fig. 4.

To illustrate the array's phase dynamics and the formation of spatially localized compartments within the transition interval, phase diagrams $(\Phi_{ij}^V,\dot{\Phi}_{ij}^V)$ are plotted in Figs. 9–11. Since the phase space of a single-junction oscillator is generically a cylinder, in all phase diagrams the right edge has to be identified with the left edge. Large dots or closed curves represent semirotations, i.e., librations, on the cylinder, while the long curves describe whirlings around it. In Fig. 9 each box represents the $(\Phi_{ij}^V,\dot{\Phi}_{ij}^V)$ phase diagram of a single junction oscillator in a 6×6 array. The numbers on the left are the values of $M|a_j|$ for the different rows. For $\beta=0.7$, $I=4.0$, and $a_j=(0.32,-0.63,-0.22,0.55,0.6,-0.07)$, there are six distinct row compartments, each of them exhibiting different spatiotemporal activity patterns. The oscillators in the rows with $j=2,4$, and 5 semirotate with very low amplitude around different nontrivial fixed points and show on the average a stationary pattern. Their first bifurcation points $M|a_j|$ lie at values just below I. In the row with $j=1$ the junction phases are in different mixed states of whirling and semirotation. All oscillators belonging to the row have the same frequency. The values of the phase slips between different oscillations in a row correspond to the values of Ψ_{ij} predicted by Eq. (21). In the rows with $j=3,6$ the couplings force the junctions into quasiperiodic oscillations.

In Figs. 10 and 11, phase diagrams of junction oscillators in selected rows are plotted. For $\beta=0.7$, $I=2.5$, and $a_1=0.9$, Fig. 10 shows an oscillator in an aperiodic mixed state of whirling and semirotation familiar from the motion of a single chaotic pendulum. The coexistence of semirotors and whirling solutions in different rows is shown in Fig. 11. For $\beta=10$, $I=2.0$, $a_1=0.4$, and $a_3=0.9$ the oscillators with $j=1$ (top) semirotate with approximately the same frequency as the quasiperiodic whirling oscillators in row number 3 (bottom).

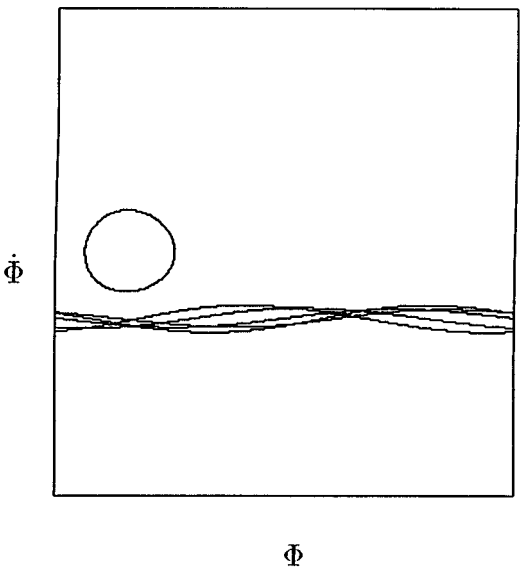

FIG. 11. Phase diagrams of two different oscillatory modes in different rows for $\beta=10$ and $I=2$. The upper oscillator semirotates with approximately the same averaged frequency as the whirling one below. The whirling oscillator is in a quasiperiodic state.

IV. DISCUSSION

We have shown that the nonlinear dynamical equations for the phases of a uniform 2D Josephson junction array with type (ii) current distribution under an external load are equivalent to an equation system for a one-dimensional chain of nonlinear, nonuniformly coupled, and nonidentical oscillators. We have determined the spatiotemporal patterns and dynamical states of the array in response to varying input patterns and coupling strengths, bias currents, and external probes. For increasing bias current the dynamics is governed by a succession of bifurcations which activate spatially distinct, coupled oscillating compartments in the array with coexisting semirotors, whirling, and quasiperiodic and aperiodic states, and which generate staircase current-voltage characteristics. These results have the following consequences.

(1) The Josephson-junction array (13) has the property that the dynamical couplings a_j in (25) and, therefore, the pattern dynamics of the array depend on and vary with the given initial conditions $\Phi_{ij}^{V}(0)=\Psi_{ij}$, i.e., on an $(N\times M)$-dimensional input pattern. This property enables the system to self-organize the stable oscillatory patterns which arise with increasing bias current. In particular, if an electron beam directed on an oscillating sample array is switched off in an LTSEM experiment, this imposes new initial conditions and a_j on the array to start with and thus generates new stable dynamical patterns. This dynamical buildup of coupling strengths due to external probes explains the succession of patterns found experimentally by Lachenmann *et al.*[16]

For dc bias currents the 2D Josephson array operates as a ''current or frequency-pattern to voltage-pattern'' transducer so that different input patterns are transformed, via $\{\Psi_{ij}\}\rightarrow\{a_j\}$, into distinct equivalence classes of observable voltage output patterns in the I-V and differential resistance characteristics, independently of phase slips and the actually very high oscillator frequencies. This is technologically relevant because the number of experimentally observed steps in the I-V characteristics is a measure for the degree of coherence of the oscillating states. If, in particular, there exists only one voltage step, then, on the subsequent linear branch of the I-V characteristics the array junctions oscillate perfectly in phase if the initial input pattern is uniform with all Ψ_{ij} being equal so that according to (21) all a_j $(j=1,\ldots,N)$ assume the same value. In the case of two or more steps coherence cannot take place. Consequently, the simplest way to achieve maximal power output consists of the application of a uniform external coherent microwave signal over the whole array. After switching this signal off, the array stores this input pattern and stays in a perfectly coherent phase-locked state. Recent experiments by Doderer and Lachenmann[20] confirm these theoretical predictions.

(2) Our theoretical analysis has shown that in a uniform 2D array current couplings alone cannot induce coherent phase locking of the junction oscillations. That all vertical and horizontal junctions cannot oscillate with the same frequency is already implicit also in Kirchhoff's voltage law. In striking contrast to this technologically unsatisfactory result we have shown in Ref. 18, both theoretically and experimentally, that in hierarchic-modular architectures of current-coupled nonlinear oscillators with $\mathbf{D}_3\times\mathbf{D}_3$ symmetry stable coherent phase-locked oscillations can be achieved with appropriately chosen couplings. Different coupling architectures can be tested in LTSEM experiments on rectangular arrays by switching distinct compartments off and on with an electron beam and measuring the increase or decrease of the coherence degree. Hybrid-modular Josephson-junction architectures with normal conducting bridges possess the additional advantage of impeding vortex propagation.

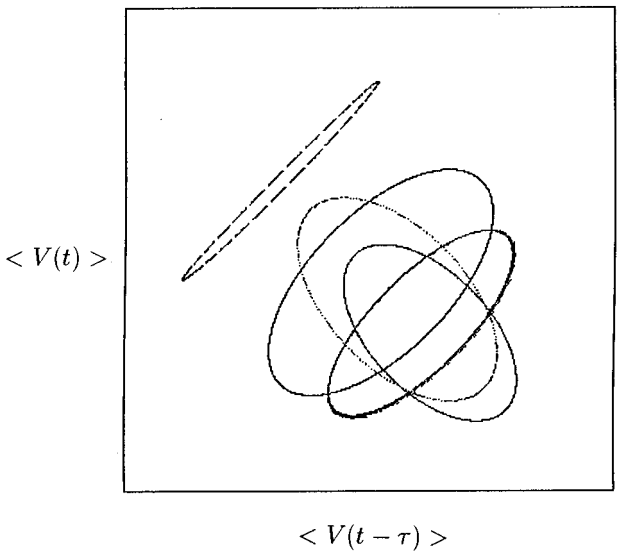

FIG. 12. Reconstruction of the array's attractors (closed curves) in the phase space of long-time averaged observables $\langle V(t-\tau)\rangle$ vs $\langle V(t)\rangle$ from numerical data obtained by simulating Eq. (13) for five different input patterns imposed on a 10×10 array. For $I=30$ the attractors generating the linear branch of the I-V characteristics can be distinguished by their positions and shapes.

(3) A novel way to determine the attractors in Josephson-junction networks from the output voltage V consists of using Takens' embedding theorem[28] for time series: For a fixed value of the bias current I_0 in the region of the linear branch of the I-V characteristics, the time variations of $V(t)$ are measured. Each input set Ψ_{ij} corresponds to a class of attractors in the phase space $V(t)$ vs $V(t-\tau)$, where τ is a given fixed time delay. Since for such high frequencies it is experimentally not possible to measure voltages time continuously, voltage was averaged in the simulations over about 10^6 oscillation periods. For $I=30$ Fig. 12 shows five different attractors of the dynamics at the linear branch in a 10×10 array for five arbitrarily chosen different input patterns. The voltage variations observed in these simulations have a magnitude of about some nV. We conclude, therefore, that Josephson networks furnish highly efficient pattern recognition devices.

(4) The dynamical equation system of a stack of 2D Josephson-junction layers (13) along the crystallographic c axis with perpendicular bias current and approximately zero voltage drop in the (a,b) direction of the layers can be transformed into a nonlinear chain equation similar to Eq. (25) with the subscript i replaced by the index pair (i,k) of the layers so that $\Phi_{ikj}^{V}(t)=\phi_j(t)+\Psi_{ikj}$. Consequently, in layered 3D Josephson-junction networks such as Bi-Sr-Ca-Cu-O crystals we find the same dynamical patterns

and switching phenomena as the ones discussed above, in particular the successive formation of compartments of oscillating junctions and the corresponding staircases for increasing bias current. Therefore, experimental data on high-T_c superconductors[5] can be interpreted in terms of the nonlinear chain of nonidentical junctions with nonuniform global couplings discussed in Sec. III. On the basis of such a chain the observed dynamical patterns find a simple and natural explanation.[19]

(5) With Eq. (8), the horizontal currents defined by (9) together with the vertical dc currents from (19), which originate from nontrivial fixed points of Eq. (13), may generate persistent circular currents of different strength and vorticity if the initial input pattern Ψ_{ij} is nonuniform [cf. Fig. 2(b)]. For small bias current, the circular currents along the edges of the array parallel to the bias current are very sensitive to external perturbations produced, e.g., by an electron beam directed on the sample, while inside the array the current distribution is able to compensate the perturbation. Using LTSEM techniques, Doderer and co-workers have imaged such pinned vortices[16] on the array edges for bias currents below the array's measured critical current. In the present theoretical framework, vortices moving through the 2D array induce voltage drops in the I-V characteristics which are in general much smaller than the step heights in the transition region and play no role in the linear branch. However, if moving vortices are interpreted as stochastic perturbations of the junctions they cross on their way through the array, our numerical simulations including parameter spreads provide strong evidence that on or near the voltage jumps, moving vortices can be responsible for the on and off switching of the corresponding array rows.

V. CONCLUSIONS

The theory presented here describes the basic nonlinear mechanisms underlying a variety of experimentally observed phenomena in Josephson-junction arrays, in particular, classical and vortex-induced row switching and voltage drops, frequency-synchronized families of phase-locked oscillators, stochastic jumps, subharmonics, and hysteresis loops in the current-voltage characteristics as a result of the intricate phase dynamics. Implications for pattern formation in high-T_c superconductors and applications in pattern recognition have been discussed and it has been shown that specific input patterns must be applied to the array or special coupling architectures be used to achieve stable coherent microwave radiation emission in 2D arrays. The theoretically predicted spatiotemporal patterns are in close agreement with the pattern dynamics observed in recent LTSEM experiments on rectangular arrays of underdamped and overdamped Josephson junctions and reproduce the measured data quantitatively.

ACKNOWLEDGMENTS

We wish to express our gratitude to T. Doderer for many stimulating discussions of his experiments. We also thank S. Lachenmann, F. Hilbert, R.P. Hübener, and J. Tomes for helpful discussions. This work was supported by the Forschungsschwerpunktprogramm des Landes Baden-Württemberg (FRG) and by the German Academic Exchange Service (DAAD). J.O. was supported by a Fellowship of the Hans-Böckler-Stiftung.

[1] T. Doderer, D. Quenter, B. Mayer, C. Krulle, A. Ustinov, R. Hübener, J. Niemeyer, R. Fromknecht, R. Poepel, U. Klein, P. Dammschneider, and J. Hinken, in *Nonlinear Superconductive Electronics and Josephson Devices*, edited by G. Costabile, S. Pagano, N. Pedersen, and M. Russo (Plenum, New York, 1991).

[2] *Nonlinear Superconducting Devices and High-T_c Materials*, edited by R.D. Parmentier and N.F. Pedersen (World Scientific, Singapore, 1995).

[3] S.P. Benz and C.J. Burroughs, Appl. Phys. Lett. **58**, 2162 (1991); P.A.A. Booi and S.P. Benz, *ibid.* **64**, 2163 (1994).

[4] D. Dominguez and J.V. José, Int. J. Mod. Phys. B **8**, 3749 (1994).

[5] R. Kleiner and P. Müller, Phys. Rev B **49**, 1327 (1994); R. Kleiner, P. Müller, H. Kohlstedt, N.F. Pedersen, and S. Sakai, *ibid.* **50**, 3942 (1994).

[6] S. Watanabe, S.H. Strogatz, H.S.J. van der Zant, and T.P. Orlando, Phys. Rev. Lett. **74**, 379 (1995).

[7] S. Watanabe and S.H. Strogatz, Physica D **74**, 197 (1994).

[8] S. Shapiro, Phys. Rev. Lett. **11**, 80 (1963); R.L. Kautz, in *Structure, Coherence and Chaos in Dynamical Systems*, edited by P. Christiansen and R.D. Parmentier (Manchester University Press, Manchester, 1989).

[9] K. Wiesenfeld, S.P. Benz, and P.A.A. Booi, J. Appl. Phys. **76**, 3835 (1994).

[10] D. G. Aronson, M. Golubitsky, and M. Krupa, Nonlinearity **4**, 861 (1991); P. Ashwin and J. W. Swift, J. Nonlinear Sci. **2**, 69 (1992).

[11] K.Y. Tsang, R.E. Mirollo, S.H. Strogatz, and K. Wiesenfeld, Physica D **48**, 102 (1991).

[12] P. Hadley, M.R. Beasley, and K. Wiesenfeld, Phys. Rev. B **38**, 8712 (1988).

[13] H.S.J. van der Zant, F.C. Fritschy, T.P. Orlando, and J.E. Mooij, Phys. Rev. B **47**, 295 (1993).

[14] J. Kim, H.J. Shin, and H.J. Lee, Phys. Rev. B **49**, 6432 (1994).

[15] W. Yu, E.B. Harris, S.E. Hebboul, J.C. Garland, and D. Stroud, Phys. Rev. B **45**, 12 624 (1992); U. Geigenmüller, C.J. Lobb, and C.B. Whan, Phys. Rev. B **47**, 348 (1993).

[16] S. Lachenmann, T. Doderer, R. Hübener, J. Niemeyer, R. Pöpel, and D. Quenter, Phys. Rev. B **48**, 3295 (1993); S.G. Lachenmann, T. Doderer, D. Hoffmann, R.P. Hübener, P.A.A. Booi, and S.P. Benz, *ibid.* **50**, 3158 (1994); T. Doderer, S.G. Lachenmann, and R.P. Hübener, in Ref. 2; S.G. Lachenmann, T. Doderer, and R.P. Hübener, in Ref. 2.

[17] T. Doderer, S.G. Lachenmann, F. Hilbert, R.P. Hübener, P.A.A. Booi, and S.P. Benz, IEEE Trans. Appl. Supercond. **5**, 2723 (1995); T. Doderer, D. Hoffmann, R. Hübener, N. Kirchmann, C. Krulle, S. Lachenmann, D. Quenter, J. Schmidt, S. Stehle, J. Niemeyer, R. Pöpel, S. Benz, and P. Booi, *ibid.* **3**, 2724 (1993).

[18] G. Dangelmayr, W. Güttinger, J. Oppenländer, J. Tomes, and M. Wegelin, Physica D (to be published).

[19] J. Oppenländer and W. Güttinger (unpublished).

[20] S.G. Lachenmann, Ph.D. thesis, University of Tübingen, 1995; S.

G. Lachenmann, T. Doderer, and R. P. Hübener, Phys Rev. B **53**, 14 541 (1996); T. Doderer, S. G. Lachenmann, and R. P. Hübener, in *Macroscopic Quantum Phenomena and Coherence in Superconducting Networks*, edited by C. Giovannella and M. Tinkham (World Scientific, Singapore, 1995).

[21] F. Hilbert, University of Tübingen, Ph.D. thesis, 1994.

[22] J.A. Sanders and R. Cushman, SIAM J. Math. Anal. **17**, 495 (1986).

[23] M. Golubitsky, B. Dionne, and I. Stewart, in *Dynamics, Bifurcations and Symmetry: New Trends and New Tools*, edited by P. Chossat (Kluwer, Dordrecht, 1994).

[24] Y. Kuramoto, *Chemical Oscillations, Waves, and Turbulence* (Springer, New York, 1984).

[25] J.D. Crawford, Phys. Rev. Lett. **74**, 4341 (1995).

[26] D. Golomb, D. Hansel, B. Shraiman, and H. Sompolinsky, Phys. Rev. A **45**, 3516 (1992).

[27] M. Octavio, in Ref. 2.

[28] F. Takens, in *Dynamical Systems and Turbulence*, edited by D.A. Rand and L.S. Young, Springer Lecture Notes in Mathematics, Vol. 898 (Springer, New York, 1980).